Experimental and numerical studies of the chromatofocusing of dilute proteins using retained pH gradients formed on a strong-base anion-exchange column

John C. Strong, Douglas D. Frey*

Department of Chemical and Biochemical Engineering, University of Maryland Baltimore County, Baltimore, MD 21228, USA

Abstract

The separation of dilute protein mixtures was achieved using simple monovalent buffering species to form retained, internally produced pH gradients on a strong-basic anion-exchange column. Highly focused proteins bands localized on stepwise pH transitions were produced experimentally under trace and volume overloaded feed conditions. Numerical simulations were performed that accurately predict the pH profile and protein band shapes in the column effluent. Experimental results were combined with numerical investigations to explore strategies for designing efficient preparative-scale chromatofocusing systems using simple, inexpensive buffers and adsorbents.

Keywords: Chromatofocusing; pH gradients; Numerical simulations; Preparative chromatography; Mobile phase composition; Adsorption equilibria; Proteins

1. Introduction

The separation of a 'target' protein from one or more impurities is of foremost concern in the preparative-scale purification of proteins as well as in analytical chromatography. Ion-exchange chromatography – a versatile separation technique capable of high resolution – has long been the mainstay of modern protein purification methods due to its simplicity, reproducibility and low cost. In the late 1970s, Sluyterman and co-workers developed a form of ion-exchange chromatography, termed chromatofocusing, which employs a retained, internally produced pH gradient [1,2]. Chromatofocusing combines the resolving power of isoelectric focusing and the simplicity of ion-exchange chromatography to yield a separation method capable of very high resolution. In addition to analytical applications, this mode of chromatography is in principle well-suited for preparative separations since it can accommodate large feed slugs (i.e., volume overloading), and since it can separate and concentrate proteins in a single step. Furthermore, among chromatographic techniques involving pH gradients, chromatofocusing tends to be the least denaturing since the method limits the amount of time proteins are exposed to pH extremes.

Despite the apparent suitability of chromatofocusing for preparative-scale separations, the current practice of the technique suffers from several limitations which hinder its use on a large scale. Perhaps the greatest limitation is the prohibitively high cost

*Corresponding author.

of the proprietary column packings and polyampholyte buffer mixtures currently used in the method. In addition, these polyampholyte buffers contain components which have been reported to associate with proteins, necessitating an additional polyampholyte removal step to recover the purified protein [3]. Moreover, polyampholyte-containing buffers produce a linear pH gradient over a wide pH range. While such a gradient is useful for analytical separations, it is not necessarily the optimal gradient shape for a preparative separation where one target protein is being separated from various contaminants in a multicomponent mixture. In order to avoid these difficulties, a number of workers have investigated the use of multicomponent mixtures of well-defined buffering species to replace the polyampholyte elution buffer in various applications of chromatofocusing (see, e.g., [4]). In particular, if a limited number of strategically chosen buffering species is employed in the elution buffer, the target protein can be eluted as a focused band on a stepwise pH transition in order to separate it from impurities which elute elsewhere on the pH gradient [5].

In previous work, a numerical method for simulating the formation of retained, stepwise pH transitions in an ion-exchange column was developed and used to investigate the focusing behavior of dilute proteins mixtures when simple buffer systems were employed [5,6]. In addition, optimized buffer compositions for producing retained pH gradients were described which eliminate the need for using a weak-base ion-exchange adsorbent having a buffering capacity. The objective of this work is to experimentally investigate the adsorption behavior of dilute protein mixtures in these types of systems, to show that experimental results from chromatofocusing experiments can be accurately simulated by numerical methods which employ independently measured physical properties, and to further develop a strategy for separating proteins with chromatofocusing using inexpensive, strong-base ion-exchange adsorbents and simple buffer mixtures.

This study investigates bivariant buffer systems where one unretained and one retained stepwise pH transitions are formed, as well as trivariant buffer systems where one unretained and two retained stepwise pH transitions are formed. Chromatofocusing with a bivariant buffer system is likely to be the preferred approach in preparative chromatography since this allows a target protein to become focused on the retained or 'slow' pH transition, while contaminants which are more weakly adsorbed than the target protein can be eluted on the unretained or 'fast' transition. Contaminants which are more strongly adsorbed than the target protein can then be eluted in a second elution step after the target protein is recovered in the column effluent. For comparison, a trivariant buffer system was also investigated in order to separate two proteins on consecutive retained pH transitions. Such systems have the advantage that both more strongly, and more weakly, adsorbed contaminants can be isolated from the target protein and eluted from the column in a single chromatofocusing procedure.

Higher-order variance systems were not investigated here since preparative separations do not typically have the objective of isolating more than one target protein, and analytical separations would normally use a linear gradient when dealing with multiple analytes. Monovariant buffer systems, such as those where sodium phosphate is used to form both the presaturation and elution buffers, were also investigated. However, such systems do not exhibit the versatility needed to perform efficient protein separations and will not be described here.

2. Basic considerations

2.1. Focusing criterion

A criterion for the focusing of protein bands in a retained pH gradient consisting of stepwise pH transitions has been discussed previously [5,6], and is illustrated graphically in Fig. 1. In particular, the figure illustrates the local-equilibrium axial pH profile in a column in terms of the velocities of the pH transitions propagating in the column. The figure applies to the case where a pH gradient is formed by presaturating an anion-exchange column at an initial pH with a buffer containing a single buffering species, and eluting the column at a lower pH using a stepwise change to an elution buffer containing a different, single buffering species. As described by Frey et al. [5], under these conditions a pH gradient is formed consisting of one unretained and one
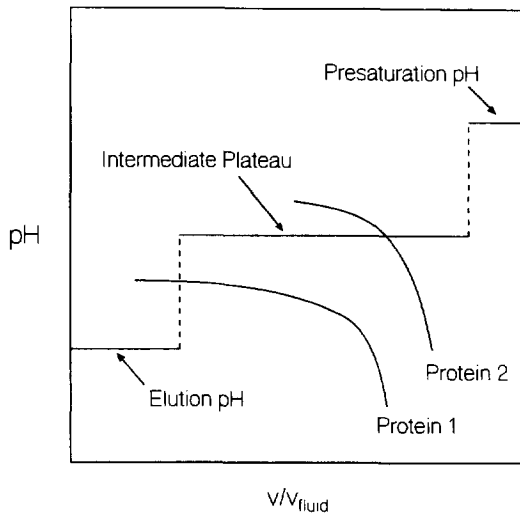
Fig. 1. Local-equilibrium behavior of a bivariant buffer system consisting of one retained and one unretained pH transition with superimposed band velocity curves of two proteins.

retained pH transition provided that both buffering species have anionic forms that participate in ion-exchange equilibrium, and if the buffering species in the presaturation buffer has a lower acid–base dissociation constant (i.e., a higher pK_a) than the buffering species in the elution buffer. Also shown in the figure are curves representing the velocities of two protein bands, which can be calculated using the following relation [7]:

$$v_{P_j} = \frac{v_{fluid}}{1 + \left(\dfrac{1-\alpha}{\alpha}\right)\epsilon_P + \dfrac{(1-\alpha)(1-\epsilon_P)}{\alpha}\left(\dfrac{q^*_{P_j,ads}}{C_{P_j}}\right)}$$

(1)

In Eq. (1), $q^*_{P_j,ads}$ denotes the equilibrium amount of protein adsorbed per unit volume of solid adsorbent when the liquid-phase protein concentration is C_{P_j}, and ϵ_P denotes the volume fraction of the particle occupied by pores accessible to the protein, as distinct from ϵ_A, which is the volume fraction of the particle occupied by pores accessible to the buffering species.

As discussed by Frey [6], if the protein band velocity curve intersects a vertical section of the pH profile (as illustrated by protein 1 in Fig. 1), the

protein experiences a focusing effect due to the fact that the protein band velocity downstream from the pH transition is less than the velocity of the transition, while the opposite situation applies upstream from the pH transition, so that the protein tends to collect at the transition itself. Conversely, when the protein band velocity curve intersects the pH profile on a plateau (as illustrated by protein 2 in Fig. 1), the protein becomes situated on the plateau and elutes from the column isocratically at that pH.

2.2. Selection of buffer system

As illustrated below, it is usually the case that the protein band velocity curve becomes relatively flat near the isoelectric point of the protein (see Fig. 9). Under these conditions, a buffer system appropriate for chromatofocusing can be approximately selected using local-equilibrium theory to ensure that a retained pH transition spans a range which includes the isoelectric point of the protein under consideration. For the relatively simple case where the presaturation and elution buffers each contain a single, different, buffering species, this condition occurs when the pH of the elution buffer, and the pH that the presaturation buffer would have if the presaturation buffering species was present at the same molar concentration as the buffering species in the elution buffer, span the appropriate pH range [6]. More complex cases, such those involving a trivariant buffer system, require an analysis which may include not only local-equilibrium theory, but also numerical calculations in order to determine the degree to which proteins become separated in the column effluent [5,6].

3. Experimental

Experiments were performed using 90-μm strong-base, anion-exchange particles (Q Sepharose FF) composed of 6% cross-linked agarose with quaternary amine groups. These particles were packed into a 26 cm × 1 cm I.D. borosilicate glass column. Either a ThermoSeparation Products SpectraSystem P4000 pump, or a fluid metering Model RP-SY pump with Model RH1CKC pump head, was used to deliver the solvent, and a ThermoSeparation Products Spec-

traSystem UV2000 UV–Vis detector monitored the absorbance of the column effluent. An Orion Model 91-03 pH minielectrode, fitted into a custom fabricated sampling cell and connected to an Orion Research Model 701A Ionalyzer, monitored the solvent pH. The analog outputs of the Ionalyzer and UV–Vis detector were directed to a STRAWBERRY TREE DATASHUTTLE, which was connected to an 80286-based IBM PS/2 computer running STRAWBERRY TREE WORKBENCH data acquisition software.

The mobile phase additives used were citric acid, obtained from J.T. Baker and sodium hydroxide, acetic acid, formic acid, N-morpholinoethanesulfonic acid (MES) and N-morpholinopropanesulfonic acid (MOPS), obtained from Sigma. All buffers were prepared by starting with a particular molar concentration of NaOH, and then adding the buffering species until the desired pH was reached. In the case of buffers containing two buffering species, one of the buffering species was first weighed out and added to the solution. The other buffering species was then added until the desired pH was achieved. All buffers were filtered with 0.2-μm Whatman Anodisc alumina matrix filter membranes and were degassed prior to use. Bovine serum albumin (BSA), bovine hemoglobin and chicken egg white ovalbumin and iron-free conalbumin were purchased from Sigma.

Chromatofocusing experiments were performed by equilibrating a 15-cm long packed bed of particles with the presaturating buffer until the column effluent reached the presaturation pH. After equilibration, a protein feed slug was loaded into the sample loop of a Rheodyne injection valve, and the solvent was switched to the eluent buffer while the protein sample was simultaneously introduced onto the column. The column effluent was monitored at 280 nm in all experiments.

4. Characterization of protein and column packing properties

4.1. Effective intraparticle protein diffusivity

In this study, the effective diffusivities of the buffering species and the hydrogen and hydroxide ions in the column packing were taken to be 0.4

times their diffusivities in the bulk liquid, as estimated from data obtained by Boyer and Hsu [8] for Sepharose CL-6B, which is similar to the column packing used in this study. However, since protein band shapes are highly dependent on the protein transport properties, intraparticle protein diffusivities in the Q Sepharose FF column packing were measured directly by applying height equivalent to a theoretical plate (HETP) analysis to pulse response experiments conducted with a trace amount of protein injected onto the column.

BSA was used as the eluate for the pulse response experiments and for convenience in interpreting the results, elution was conducted isocratically at a low pH such that BSA was positively charged and therefore unretained by the anion-exchange adsorbent. This procedure was presumed to be the most consistent way to conduct the experiments since the alternative of using high ionic strengths could have introduced errors associated with hydrophobic interactions and with swelling effects associated with the column packing. Although BSA has been reported to exhibit electrostatic binding to ion-exchange adsorbents at pH values lower than its isoelectric point for certain conditions [9], this type of behavior was not apparent here. In particular, the retention time of BSA observed in these experiments corresponds to the value expected from assuming the interparticle and particle porosities were 0.35 and 0.52, respectively, the former being the value generally expected for a packed bed of particles, while the latter is nearly the same as the particle volume fraction accessible to BSA reported for Sepharose CL-6B [8]. In addition, the retention time measured for BSA was nearly the same as the retention time for conalbumin measured at the same flow-rate using a high ionic strength eluent which should have yielded no retention of this protein, i.e., 2.0 M NaCl at pH 6.0.

The first absolute and second central moments of the Gaussian peaks resulting from the pulse response experiments were measured, and the reduced plate height (i.e., $h = H/d_p$) was determined using the relation

$$h = \frac{\sigma^2 L}{d_P \, t_{m^2}} \qquad (2)$$

In the case where axial molecular diffusion and the

external resistance to mass transfer are negligible contributions to band spreading, the expression for the reduced plate height takes the form [10]

$$h = \frac{2D_{AD}}{v_{fluid}\, d_P}$$
$$+ \left[\frac{\alpha d_p (k'(\alpha(1-\epsilon_p)+\epsilon_p)+\epsilon_p(1-\alpha))^2 v_{fluid}}{30(1-\alpha)(k'+1)^2(\alpha(1-\epsilon_p)+\epsilon_p)^2} \right]$$
$$\times \left(\frac{1}{D_{eff}} \right) \qquad (3)$$

The first term on the right side of Eq. (3) accounts for the axial dispersion and extracolumn band broadening contribution to the reduced plate height (h_{AD}), and is written in terms of a lumped axial dispersion coefficient (D_{AD}) which incorporates both effects. This term tends to be independent of the flow rate and is therefore a fixed constant for a given column. Axial dispersion and extracolumn band broadening can also be expressed in terms of a lumped axial dispersion Peclet number given by $Pe_{AD} = 2/h_{AD}$. The second term on the right side of Eq. (3) is linear in the interstitial fluid velocity so that a plot of h versus v_{fluid} will produce a straight line, the slope of which is related to D_{eff}, while the intercept yields the value of h_{AD}.

Protein chromatography is typically conducted at fluid velocities large enough so that the first term in Eq. (3) is relatively small in comparison with the other term. If the first term in Eq. (3) is neglected (i.e., if axial dispersion is neglected), the resulting material-balance equations describing transport in a packed bed are hyperbolic in nature, and therefore amenable to numerical integration by the method of characteristics [11]. Since the simulations employed in this study utilize this numerical technique, the relatively minor effects of axial dispersion and extracolumn band broadening were accounted for by modifying Eq. (3) so that it has a zero intercept, but still yields the appropriate value of h for a particular value of v_{fluid}. In this way, D_{AD} and D_{eff} can be combined into an overall diffusion coefficient, D_c, given by

$$D_c = \left(\frac{1}{D_{eff}} + \frac{2}{A\, Pe_{AD}} \right)^{-1} \qquad (4)$$

where A denotes the quantity in square brackets on the right side of Eq. (3). Eq. (4) is similar to other relations proposed for combining the effects of axial dispersion and intraparticle diffusivity into a single transport parameter [12]. Although Eq. (4) was developed for the case of linear equilibrium, it will also be used to account for the effect of axial dispersion on the behavior of the buffering species, even though these species exhibit nonlinear adsorption equilibrium under the conditions employed here. For the purpose of this approximation, the quantity A will be evaluated in the limit $k' \rightarrow \infty$ due to the fact that the liquid-phase concentrations of the buffering species are relatively small so that these species tend to have a large adsorption equilibrium distribution coefficient.

Fig. 2 shows experimentally measured reduced plate heights for BSA as a function of reduced velocity. Although the main objective of this work is to numerically simulate the chromatofocusing behavior of BSA, the intraparticle diffusion coefficients for conalbumin and ovalbumin were also determined for comparison using similar methods. Linear regression was used to determine the best fit to the data, and the resulting effective diffusion coefficients are listed in Table 1.

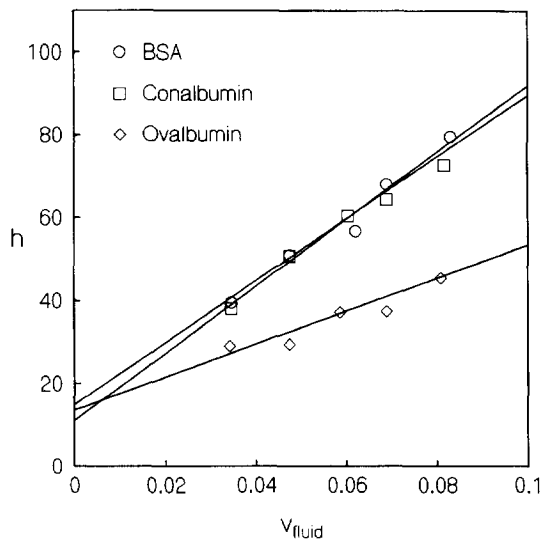The contribution to the plate height due to axial

Fig. 2. Experimentally determined dependence of reduced plate height on mobile phase fluid velocity. Experiments were performed with a 0.1-ml feed slug containing 0.1 mg ml^{-1} protein and with a buffer consisting of 0.071 M citrate at pH 3.5.

Table 1

Protein	M_r	D_{eff} (cm^2 s^{-1})
Ovalbumin	$43.5 \cdot 10^3$	$1.15 \cdot 10^{-7}$
Conalbumin	$67.0 \cdot 10^3$	$4.60 \cdot 10^{-8}$
BSA	$77.0 \cdot 10^3$	$4.74 \cdot 10^{-8}$

dispersion and extracolumn band broadening is given by the intercept of the data in Fig. 2, where it can be seen that $h_{AD} \approx 13$, which corresponds to $Pe_{AD} \approx 0.15$. According to Miller and King [13], axial dispersion in a bed of spherical particles at low Reynolds numbers is described by the relation $\alpha Pe_{AD} \approx 0.20$ or, since $\alpha \approx 0.34$ for a well-packed bed, by $Pe_{AD} \approx 0.6$. The value of Pe_{AD} observed in this study was substantially smaller than this, which is likely due to the fact that extracolumn band broadening was largely avoided in the experimental apparatus of Miller and King, whereas in the apparatus used here this effect tends to be more significant. However, the amount of axial dispersion and extracolumn band broadening observed in this study is similar to that observed by Boyer and Hsu [8] who used short columns packed with 110 μm diameter particles and obtained $h_{AD} = 11.6$, which corresponds to $Pe_{AD} = 0.17$.

The effective diffusion coefficients for the three proteins shown in Table 1 are consistent with trends expected from their respective sizes. For example, the Stokes–Einstein equation [14] predicts that the ratio of bulk-liquid diffusion coefficients for BSA and ovalbumin is 1.2, based on their respective average diameters. The higher diffusivity ratio of 2.4 observed for these proteins in Table 1 is likely due to the additional frictional hindrance caused by the pore walls in the particles constituting the column packing. Due to its larger size and ellipsoid shape, this effect would be expected to be more pronounced for BSA than for ovalbumin, which presumably accounts for the greater ratio of effective diffusion coefficients. After correcting the diffusion coefficients observed here for the effect of temperature using the Stokes–Einstein equation, it was determined that these diffusivities were slightly less than those obtained by Boyer and Hsu [8] for Sepharose CL-6B.

4.2. Determination of adsorption equilibrium parameters

In addition to mass-transfer properties, the equilibrium adsorption properties of the proteins must also be characterized in order to predict their chromatographic behavior. If the adsorbed and liquid phases are in equilibrium, the chemical potential of electrically neutral pairs of ions is the same in both phases. Since the hydrogen ion is always present in both phases, it is convenient to use this ion to write equilibrium expressions as follows [5]:

$$(q_{H^+,ads}^*)^{-z_{A_i^-}} q_{A_i^-,ads}^* = K_{A_i^-,ads} (C_{H^+})^{-z_{A_i^-}} C_{A_i^-} \quad (5a)$$

$$(q_{H^+,ads}^*)^{-z_{A_i^0}} q_{A_i^0,ads}^* = K_{A_i^0,ads} (C_{H^+})^{-z_{A_i^0}} C_{A_i^0} \quad (5b)$$

$$(q_{H^+,ads}^*)^{-z_{A_i^+}} q_{A_i^+,ads}^* = K_{A_i^+,ads} (C_{H^+})^{-z_{A_i^+}} C_{A_i^+} \quad (5c)$$

$$(q_{H^+,ads}^*)^{-z_{P_j}} q_{P_j,ads}^* = K_{P_j,ads} (C_{H^+})^{-z_{P_j}} C_{P_j} \quad (5d)$$

where A_i^-, A_i^0 and A_i^+ denote the negatively charged, uncharged and positively charged forms of the buffering species A_i. Note that, since $z_{A_i^0} = 0$, Eqs. (5b) yields the result $q_{A_i^0,ads} = K_{A_i^0,ads} C_{A_i^0}$. In addition, Eqs. (5a) and Eqs. (5d) can be combined to yield an expression describing stoichiometric ion exchange as follows:

$$\left(\frac{q_{A_i^-,ads}^*}{C_{A_i^-}}\right)^{z_{P_j}} = \left[\frac{K_{A_i^-,ads}^{z_{P_j}}}{K_{P_j,ads}^{z_{A_i^-}}}\right] \left(\frac{q_{P_j,ads}^*}{C_{P_j}}\right)^{z_{A_i^-}} \quad (6)$$

For a dilute protein, the retention factor k' is defined as the ratio of the amount of solute adsorbed to that in the mobile phase according to

$$k' = \frac{\bar{n}_j}{n_j} = \frac{(t_m - t_0)}{t_0} = \frac{(1-\alpha)(1-\epsilon_P)}{\alpha + (1-\alpha)\epsilon_P}\left(\frac{q_{P_j,ads}^*}{C_{P_j}}\right) \quad (7)$$

Furthermore, for a dilute protein the approximation $q_{A_i^-,ads}(1 - \epsilon_A) = q_R$ applies, where q_R is the number of moles of charged functional groups on the adsorbent per unit volume of particle. In this case, Eq. (7) can be combined with Eqs. (5a–5d) and (6) to arrive at the following linear relation between the capacity factor and the concentration of A_i^-:

$$\log(k') = \log(\phi_{\mathrm{P}} \, K_{\mathrm{P_j,ads}})$$

$$+ \, z_{\mathrm{ij}} \, \log\!\left(\frac{q_{\mathrm{R}}}{K_{\mathrm{A_i^-,ads}} \, (1 - \epsilon_{\mathrm{A}}) \, C_{\mathrm{A_i^-}}} \right) \quad (8)$$

In Eq. (8), $z_{\mathrm{ij}} = z_{\mathrm{P_j}}/z_{\mathrm{A_i^-}}$, and ϕ_{P} is the phase ratio for the protein.

Although the preceding development yields relations similar to those commonly used by other investigators to represent protein ion-exchange equilibrium (see, e.g., [9]), Eq. (5d) exhibits the characteristic that $q_{\mathrm{P_j,ads}}^* = K_{\mathrm{P_j,ads}} \, C_{\mathrm{P_j}}$, rather than the expected value of zero, when $z_{\mathrm{P_j}} = 0$ is substituted into that equation. This is due to the fact that the adsorption equilibrium constant in Eq. (5d) is assumed to be independent of the protein charge, in which case that equation predicts that the amount adsorbed of an uncharged protein is linearly related to its liquid-phase concentration. The remainder of this section describes an alternative formulation of the equilibrium relations that eliminates this feature while still accurately fitting protein adsorption data. Furthermore, as discussed below, this alternative formulation is more readily incorporated into the numerical procedures for calculating adsorption dynamics described by Frey et al. [5].

It is sometimes convenient to express protein adsorption empirically in terms of the total amount of protein present in the particle per unit volume of particle (see, e.g., [5,15]). For this purpose, equilibrium constants based on the total amount of a species present in the particle can be defined as

$$(q_{\mathrm{H^+}}^*)^{-z_{\mathrm{A_i^-}}} \, q_{\mathrm{A_i^-}}^* = K_{\mathrm{A_i^-,t}} \, (C_{\mathrm{H^+}})^{-z_{\mathrm{A_i^-}}} \, C_{\mathrm{A_i^-}} \quad (9\mathrm{a})$$

$$(q_{\mathrm{H^+}}^*)^{-z_{\mathrm{A_i^0}}} \, q_{\mathrm{A_i^0}}^* = K_{\mathrm{A_i^0,t}} \, (C_{\mathrm{H^-}})^{-z_{\mathrm{A_i^0}}} \, C_{\mathrm{A_i^0}} \quad (9\mathrm{b})$$

$$(q_{\mathrm{H^+}}^*)^{-z_{\mathrm{A_i^+}}} \, q_{\mathrm{A_i^-}}^* = K_{\mathrm{A_i^+,t}} \, (C_{\mathrm{H^-}})^{-z_{\mathrm{A_i^+}}} \, C_{\mathrm{A_i}}^+ \quad (9\mathrm{c})$$

$$(q_{\mathrm{H^+}}^*)^{-z_{\mathrm{P_j}}} \, q_{\mathrm{P_j}}^* = K_{\mathrm{P_j,t}} \, (C_{\mathrm{H^+}})^{-z_{\mathrm{P_j}}} \, C_{\mathrm{P_j}} \quad (9\mathrm{d})$$

where concentrations per unit volume of particle are given by

$$q_{\mathrm{A_i^-}}^* = (1 - \epsilon_{\mathrm{A}}) q_{\mathrm{A_i^-,ads}}^* + \epsilon_{\mathrm{A}} C_{\mathrm{A_i^-}} \quad (10\mathrm{a})$$

$$q_{\mathrm{P_j}}^* = (1 - \epsilon_{\mathrm{P}}) q_{\mathrm{P_j,ads}}^* + \epsilon_{\mathrm{P}} C_{\mathrm{P_j}} \quad (10\mathrm{b})$$

with similar relations applying to the uncharged and positively charged forms of A_i. The velocity of a protein band is then given by

$$v_{\mathrm{P_j}} = \frac{v_{\mathrm{fluid}}}{1 + \left(\dfrac{1 - \alpha}{\alpha} \right) \dfrac{q_{\mathrm{P_j}}^*}{C_{\mathrm{P_j}}}} \quad (11)$$

Using assumptions similar to those that led to Eq. (8), Eq. (7) can be combined with Eqs. (9a–9d), (10a) and (10b) to yield

$$\log\!\left(k' + \frac{\epsilon_{\mathrm{p}} \phi_{\mathrm{p}}}{1 - \epsilon_{\mathrm{p}}} \right) = \log\!\left(\frac{\phi_{\mathrm{P}} \, K_{\mathrm{P_j,t}}}{1 - \epsilon_{\mathrm{p}}} \right)$$

$$+ \, z_{\mathrm{ij}} \, \log\!\left(\frac{q_{\mathrm{R}}}{K_{\mathrm{A_i^-,t}} \, C_{\mathrm{A_i^-}}} + \frac{\epsilon_{\mathrm{A}}}{K_{\mathrm{A_i^-,t}}} \right) \quad (12)$$

In contrast to Eqs. (5a–5d), it can be seen that Eqs. (9a–9d) are consistent with the requirement of an ion-exchange isotherm that $q_{\mathrm{P_j,ads}}^* = 0$ when $z_{\mathrm{P_j}} = 0$. In particular, Eq. (12) indicates that adsorption behavior can be accounted for when k' approaches zero (i.e., when z_{ij} approaches zero) by setting $K_{\mathrm{P_j,t}} = \epsilon_{\mathrm{p}}$. Since the use of Eqs. (9a–9d) also simplifies the numerical calculations described by Frey et al. [5] by eliminating the need to calculate the composition of the fluid in the particle pores, these equations will be used in the remainder of this study to represent adsorption behavior in the range $z_{\mathrm{ij}} > 0$. Furthermore, when $z_{\mathrm{ij}} < 0$ and an ion-exchange mechanism no longer applies, the amount adsorbed corresponding to $z_{\mathrm{ij}} = 0$ will be employed, i.e., $q_{\mathrm{P_j}}^* = K_{\mathrm{P_j,t}} C_{\mathrm{P_j}}$. As demonstrated below, this approach is able to fit experimental data for the adsorption of BSA on Q Sepharose FF at least as well as when Eqs. (5a–5d) are employed over the full range of z_{ij}.

To determine the adsorption equilibrium constants defined by Eqs. (9a–9d), a trace quantity of protein was eluted isocratically in a column packed with Q Sepharose FF using consecutively higher ionic strength eluents. These experiments were then repeated for a range of eluent pH values. According to Eq. (12), $K_{\mathrm{P_j,t}}$ can be obtained from the intercept of the line formed when the logarithmic term on the left side of Eq. (12) is plotted as a function of the second

logarithmic term on the right side of Eq. (12), while the dependence of z_{ij} on the mobile phase pH can be determined by the slope of this line.

Fig. 3 summarizes retention data for BSA at several values of liquid phase pH and ionic strength with acetic acid as the buffering species. To arrive at the capacity factor [i.e., $(t_m - t_0)/t_m$], the retention time of an unadsorbed eluate was determined from the retention time of BSA under non-binding conditions as discussed earlier, and k' was then determined at each ionic strength. As shown in Fig. 3, in the pH range from 5.0–6.5 the retention data for BSA is consistent with Eq. (12). The fitting of the data in Fig. 3 was accomplished by setting $K_{P_j,t} = \epsilon_p$ with the value of ϵ_p determined in the previous section, and then selecting a value for $K_{A_i^-,t}$ and a value for z_{ij} for each pH in order to minimize the discrepancy between experimental data and Eq. (12). Although it might be expected that the values of the physical properties used to fit the experimental data in Fig. 3 would vary somewhat with pH and ionic strength, as shown in the figure single average values for these parameters were able to accurately fit these
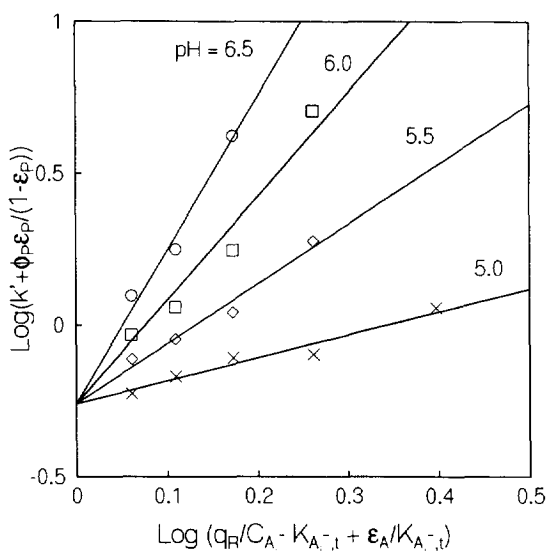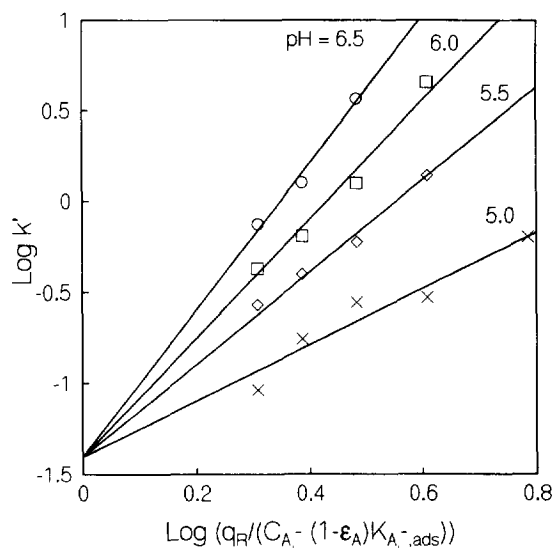

Fig. 4. Retention data obtained using acetate buffers to determine the characteristic protein binding charge as a function of pH, and the adsorption equilibrium constant for BSA using Eq. (8) and the equilibrium adsorption constants defined by Eqs. (5a), (5b), (5c), (5d). Calculated lines correspond to $K_{P_j,ads} = 0.086$, $K_{A_i^-,ads} = 2.87$, $\epsilon_p = 0.52$, $\epsilon_A = 0.8$, $\alpha = 0.34$, $q_R = 0.35$ mol/l and $z_{ij} = 4.0$, 3.3, 2.5, and 1.5 (top to bottom). Flow-rates varied from 0.8–1.2 ml/min.

data in the range of conditions investigated. For comparison, Fig. 4 illustrates the use of Eq. (8) to fit experimental data for BSA adsorption on Q Sepharose FF. As shown, the data is represented by Eq. (12) at least as well as it is by Eq. (8), which justifies the use of the equilibrium relations defined by Eqs. (9a–9d) in this study.

Figs. 3 and 4 indicate that the experimental retention data for a given pH tend to have a slope which decreases slightly with the ionic strength, at least for the three higher pH values shown in the figures. One likely reason for this trend is the fact that the effective pH in the anion-exchange adsorbent is generally less than that in the adjacent fluid phase [16], so that the measured characteristic binding charge represents an average of the charges that exist on the protein binding region in the fluid and adsorbed phases. Furthermore, at low ionic strength there is a decreased amount of hydrogen ion uptake by Donnan equilibrium as compared to the case of high ionic strength. This implies that the effective pH in the adsorbent decreases as the ionic strength
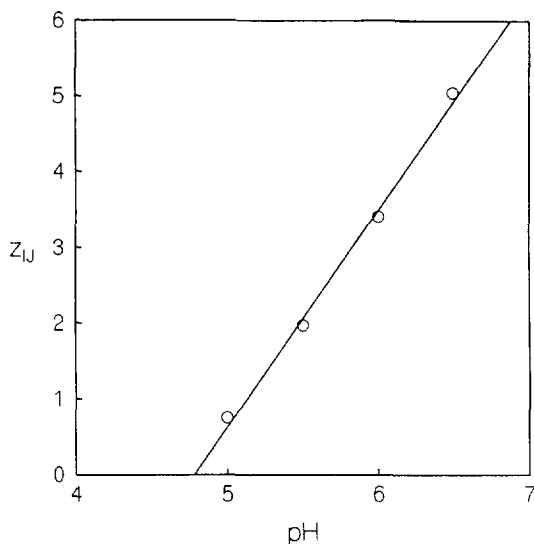

Fig. 3. Retention data obtained using acetate buffers to determine the characteristic protein binding charge as a function of pH and the equilibrium adsorption constants defined by Eq. (11). Calculated lines correspond to $K_{P_j,t} = 0.52$, $K_{A_i^-,t} = 1.65$, $\epsilon_p = 0.52$, $\epsilon_A = 0.8$, $\alpha = 0.34$, $q_R = 0.35$ mol/l and $z_{ij} = 5.1$, 3.4, 2.0, and 0.8 (top to bottom). Flow-rates varied from 0.8–1.2 ml/min.

Fig. 5. Characteristic charge for BSA as a function of pH obtained from data in Fig. 3. Fitted line corresponds to $pH_{rcf} = 4.7$ and $a_p = 2.6$.

increases, which likely accounts for the curvature of the retention data observed in Figs. 3 and 4.

Fig. 5 illustrates the relation between the mobile phase pH and the characteristic binding charge for BSA determined from Fig. 3. As shown, the relationship is linear in the pH range investigated. The characteristic binding charge for BSA shown in Fig. 5 can be compared to its total titrametric charge, which varies from zero at pH 4.8 to −15 at pH 7 [17]. This indicates that approximately one third of the functional groups on BSA which are titrated in this pH range are involved in the adsorption process. For simplicity, it will be assumed that z_{ij} is a function of the liquid phase pH (rather than the adsorbed phase pH) and, since it appears that the characteristic binding charge is generally a linear function of the liquid phase pH when this charge is moderate in value [9], the following relation will be employed:

$$z_{ij} = a_{P_j} (pH_{ref} - pH) \qquad (13)$$

Data of the type just described were not obtained for hemoglobin and conalbumin, which were the two other proteins used in this study. Instead, the equilibrium adsorption properties for these two proteins

were estimated from data in the literature [9]. For this reason, experimental data for the elution of BSA will be used to demonstrate that numerical simulations are able to predict column performance quantitatively when the equilibrium and transport parameters characterizing BSA are measured independently. In contrast, experimental data for hemoglobin and conalbumin are used primarily to compare the elution behavior of different proteins on a more qualitative basis.

Values for $K_{A_i^-,t}$ for MES, acetic acid, and formic acid were obtained by comparing the experimental pH profile with numerical calculations for the case where the column was presaturated at a low pH with one buffering species, and eluted at a high pH with another buffering species. Under these conditions, the effluent pH profile consists of a relatively steep, unretained transition corresponding to a change in the liquid-phase concentration of the presaturation buffering species, followed by a retained, non-self-sharpening transition which is relatively broad and which corresponds to the ion exchange of buffering species. For such a profile, the position of the unretained front is mainly determined by the adsorption equilibrium constant of the neutral form of the presaturation buffering species (i.e., $K_{A_i^0,t}$), while the shape of the retained front is mainly determined by the adsorption equilibrium constants for the two exchanging ionic species. More specifically, the ratio of the adsorption equilibrium constants for the anionic forms of the buffering species primarily determines the shape of the retained front while the absolute values of these constants for a given ratio is of less importance since there is relatively little adsorption of neutral salts on this transition.

Fig. 6 illustrates a comparison of the calculated and experimentally measured effluent pH profiles for a column employing a formate–acetate buffer system where the presaturation and elution conditions were chosen as just described. As shown, good agreement between experimental data and calculated results was achieved by setting $K_{A_i^-,t} = 2.6$ and 1.68 for formic and acetic acids, respectively, and with the other adsorption equilibrium constants (i.e., $K_{A_i^0,ads}$) as described in the figure caption. Similarly, Fig. 7 shows experimental data and numerical calculations for the particular values of $K_{A_i^-,t}$ that yield the best agreement between data and calculations for the
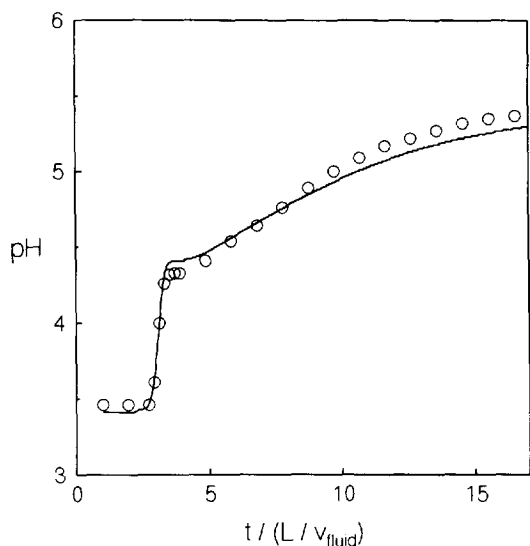
Fig. 6. Experimental data and numerical calculations of pH gradient for a column packed with 90 μm Q-Sepharose FF presaturated at pH 3.5 with 0.178 M formic acid and eluted at pH 5.5 with 0.0625 M acetic acid at a flow-rate of 0.85 ml min^{-1}. Calculations correspond to $\alpha = 0.35$, $q_R = 0.35$ mol l^{-1}, and $K_{A_j^-,t} = 1.65$ and 2.6, and $K_{A_j^0,t} = 1.0$ and 1.05, for acetic and formic acid, respectively.
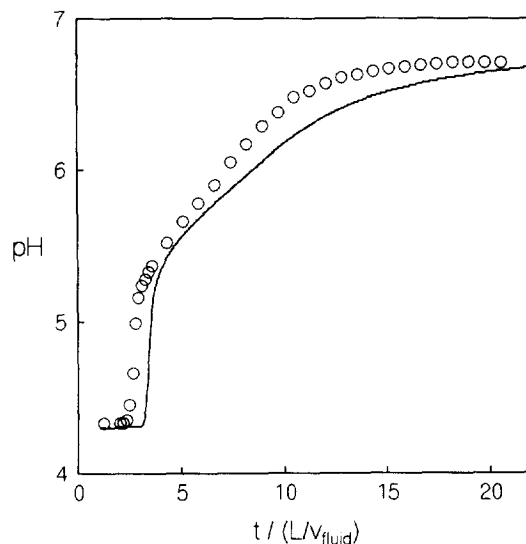
Fig. 7. Experimental results and numerical calculations of effluent pH profile for a column packed with 90 μm Q-Sepharose FF presaturated at pH 4.3 with 0.19 M acetic acid and eluted at pH 6.7 with 0.065 M MES at a flow-rate of 0.85 ml min^{-1}. Calculations correspond to $\alpha = 0.35$, $q_R = 0.35$ mol l^{-1}, and $K_{A_j^-,t} = 1.65$ and 1.0, and $K_{A_j^0,t} = 1.26$ and 0.8, for acetic acid and MES, respectively.

effluent pH profile from a column employing a MES–acetate buffering system.

5. Chromatofocusing results and discussion

5.1. Separation of focused and unfocused proteins

Fig. 8 shows experimental results and a numerical calculation of the chromatofocusing of BSA and hemoglobin using a MES–acetate buffer system where the column was presaturated at a high pH and eluted at a low pH, and where both proteins were introduced into the column in a 0.1-ml injection slug at a concentration of 1 mg ml^{-1}. The numerical calculations were performed using the method of characteristics as described by Frey et al. [5]. As shown, good agreement was obtained between experimental data and numerical calculations under these conditions.

One feature of both the experimental and numerically calculated pH profiles in Fig. 8 is that the second pH transition to exit the column is much

steeper than the first. As discussed by Frey et al. [5,6], this is due to the fact that the first transition is unretained by the column since it is associated with a change in the liquid-phase concentration of MES without any change in the adsorbed-phase composition. This transition therefore exhibits the square-root broadening behavior characteristic of linear adsorption equilibrium. The retained transition, however, is formed by the exchange of MES and acetate ions under constant-pattern conditions, and therefore exhibits self-sharpening behavior which leads to a steeper transition.

The pH profile for the MES–acetate just described, and the pH profile for an analogous acetate–formate buffer system, are shown in Fig. 9. In particular, the figure illustrates the experimentally determined velocities of the various pH transitions, but with the transitions represented as stepwise changes as would occur under local-equilibrium conditions. Also shown in the figure is the band velocity curve for BSA calculated from Eq. (1) using the equilibrium constants defined by Eqs. (5a–5d), and the same curve calculated from Eq. (11) using
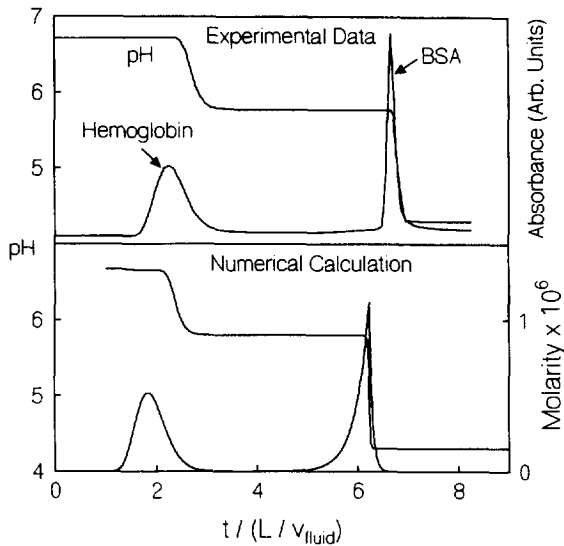
Fig. 8. Experimental data and numerical calculations for the chromatofocusing of hemoglobin and BSA. Experiments employed a 0.065 M MES presaturation buffer at pH 6.7, a 0.19 M acetic acid elution buffer at pH 4.3, a 15-cm length particle bed containing 90 μm Q-Sepharose FF, a flow-rate of 0.91 ml min^{-1} and a 0.1 ml feed slug containing 1.0 mg ml^{-1} of both proteins. Calculations employ the equilibrium adsorption and transport properties for BSA and the buffering species determined in Figs. 2–7 together with $D_{AD} = 3.3 \cdot 10^{-3}$ cm^2 s^{-1}, as determined from the value of h_{AD} in Fig. 2. Properties for hemoglobin were inferred from data given in Hearn et al. [9] and correspond to $K_{P_{j,1}} = 0.52$, $a_p = 1.93$, pH$_{ref} = 6.7$, $D_{eff} = 7.0 \cdot 10^{-8}$ cm^2 s^{-1}.
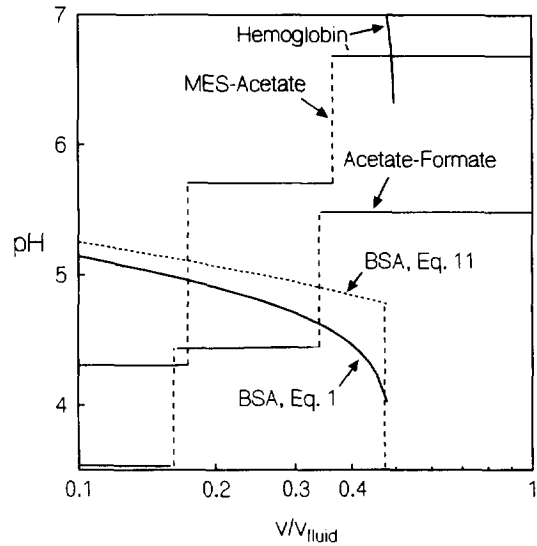

Fig. 9. Local-equilibrium pH profiles for MES–acetate and acetate–formate buffer systems superimposed on the band velocity curves for BSA and hemoglobin. The acetate–formate buffer system corresponds to presaturating the column at pH 5.5 with 0.0625 M acetic acid and eluting the column at pH 3.5 with 0.178 M formic acid while the MES–acetate buffer system is the same used in Fig. 8. The band velocity curve for BSA was calculated using both Eqs. (1), (11) with the parameters determined in Figs. 3 and 4. The parameters needed to determine the band velocity curve for hemoglobin were inferred from data in Hearn et al. [9] (see caption to Fig. 8).

the equilibrium constants defined by Eqs. (9a–9d). Since a protein will participate in ion-exchange equilibrium with different ionic species on the upstream and downstream sides of a retained transition, an average of the adsorption equilibrium constants for the various buffering species was used when determining the band velocity curves shown in the figure in order to simplify the calculations. As discussed previously, when using the equilibrium constants defined by Eqs. (9a–9d), it was assumed that $q_{P_j}^* = K_{P_{j,1}} C_{P_j}$ when $z_{ij} < 0$, which accounts for the vertical decrease in the band velocity curve shown at the pH where $z_{ij} = 0$.

The band velocity curves for BSA in Fig. 9 calculated by either Eq. (1) or Eq. (11) intersect the MES–acetate pH profile on the retained pH transition, which indicates that BSA will elute from the column as a focused band on that transition. Furthermore, the steepness with which the band velocity

curve of BSA intersects the vertical pH transition can be taken as a qualitative indication of the strength of the focusing effect. In particular, when the band velocity curve intersects the vertical pH transition at a shallow angle, the large sensitivity of the band velocity to pH causes the protein to become strongly focused on the transition since there is a large difference in protein band velocities on the pH plateaus adjoining the transition. Conversely, when the band velocity curve is steep near its intersection with the vertical section of the pH profile, there is a weaker focusing effect and the band width of the focused protein is greater since there is a smaller difference in protein band velocities on the pH plateaus adjoining the transition.

Although the fast transitions for both buffer systems depicted in Fig. 9 are not produced by ion exchange and are therefore unretained by the column, they nevertheless are able to travel substantially slower than the velocity of an unretained protein.

In particular, the experimentally determined velocities for the fast transitions in Fig. 9 are less than the velocity of an unretained protein due to the adsorption of the uncharged form of the buffering species present on that transition, and because the pore volume accessible to a buffering species is greater than that accessible to a protein as a result of the larger size of the latter. For these reasons, it is possible for a protein band to overtake the fast pH transitions shown in the figure, in which case the band velocity curve of a weakly adsorbed protein can intersect and become focused on those transitions. These conditions are illustrated by the behavior of BSA in the acetate–formate buffer system in Fig. 9, and confirmed by the corresponding experimental results shown in Fig. 10. Fig. 9 also illustrates the fact that the protein band velocity curve generally becomes steeper with increasing band velocity, so that focusing effects are generally weaker on the first eluting transition as compared to the second transition. This trend is also apparent when comparing Figs. 8 and 10, where it is observed that the band width of BSA is smaller when it is focused on the retained transition.

In contrast to the case for BSA, Fig. 8 indicates that hemoglobin elutes isocratically on the presaturant pH plateau. This agrees with the observations of Hearn et al. [9] who found that hemoglobin exhibits a characteristic binding charge of -5 at a mobile phase pH of 9.6, but that the characteristic charge becomes nearly zero at a pH of 7.5. The band velocity curve for hemoglobin, estimated from the data of Hearn et al. [9], is also shown in Fig. 9, and is consistent with the location of hemoglobin on the pH profile. In order to calculate the band shape for hemoglobin in Fig. 8, it was assumed that $pH_{ref} = 7.5$, so that $q_{P_j}^* = K_{P_j,t} C_{P_j}$ on the presaturation plateau.

5.2. Separation of two focused proteins

A trivariant buffer system consisting of MOPS, MES and acetic acid was used to investigate the behavior of a chromatofocusing system where two proteins are separated on adjacent retained pH transitions. To conduct the experiments, the column was presaturated with a buffer containing MOPS at pH 8.0, and then eluted with a buffer containing MES and acetic acid at pH 4.3. BSA and conalbumin were introduced into the column in a 1.0 ml feed slug at a concentration of 1.0 mg ml^{-1}. Experimental results and numerical simulations corresponding to this procedure are illustrated in Fig. 11.

The final transition to exit the column in Fig. 11 is created by the exchange of MES and acetate ions, and exhibits behavior similar to the retained transition in Fig. 8 since it spans the pH at which the characteristic charge of BSA becomes zero. As shown, BSA is again focused into a band on this transition, although in this case an unidentified shoulder peak was present on the same transition. Conalbumin elutes on the middle pH transition, which is formed by the ion exchange of MOPS and MES ions, and which spans a pH range from 5.60 to 6.65. Since the isoelectric point of iron-free conalbumin is 6.73 [18], it appears that for conalbumin the titrametric charge is not an accurate indicator of the characteristic binding charge since this protein adsorbs onto the column packing in significant amounts at a pH below its isoelectric point. In order to simulate the band shape for conalbumin shown in
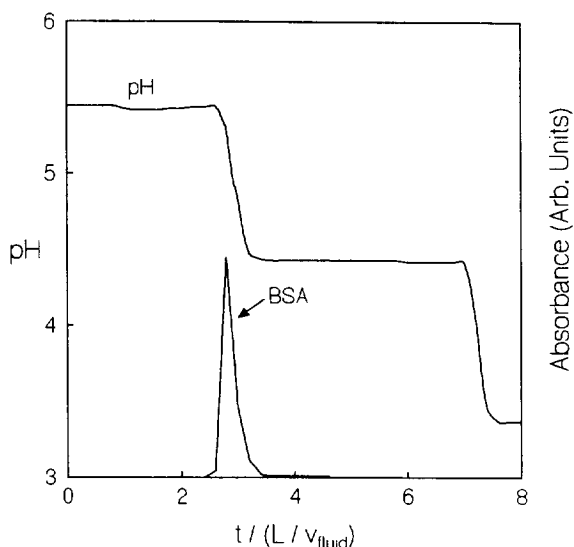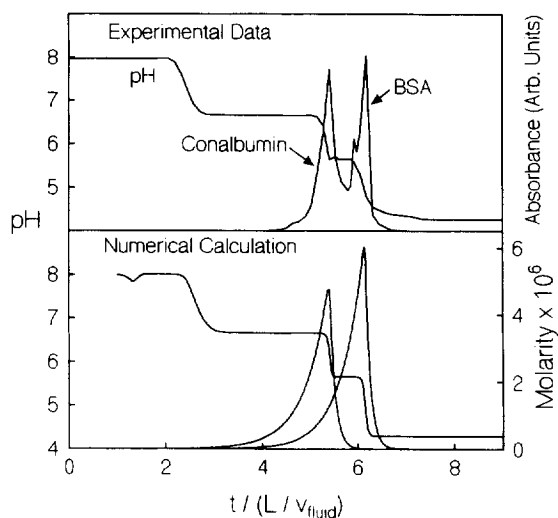

Fig. 10. Experimental data for the chromatofocusing of BSA for the case where the column was presaturated with the acetate–formate buffer system described in the caption to Fig. 9. Experiments employed a 15-cm length particle bed containing 90 μm Q-Sepharose FF, a flow-rate of 1.0 ml min^{-1}, and a 0.1-ml slug size containing 1.0 mg ml^{-1} of BSA.

Fig. 11. Experimental data and numerical calculations for the chromatofocusing of conalbumin and BSA. Experiments employed a 0.058 M MOPS presaturation buffer at pH 8.0, an elution buffer containing 0.04 M MES and 0.19 M acetic acid at pH 4.3, a 15-cm length particle bed containing 90 μm Q-Sepharose FF, a flow-rate of 1.32 ml min^{-1}, and a 1.0-ml slug size containing 1.0 mg ml^{-1} of both proteins. Calculations employ the equilibrium adsorption properties determined in Figs. 2–7 and $D_{AD}=4.7\cdot10^{-3}$ cm^2 s^{-1}, as determined from the value of h_{AD} in Fig. 2. $K_{A^-,t}$ and $K_{A^0,t}$ were set equal to unity for MOPS. Properties used for the calculation of the conalbumin elution profile were $K_{P,t}=0.52$, $a_p=2.2$, pH$_{ref}=6.0$, and $D_{eff}=4.6\cdot10^{-8}$ cm^2 s^{-1}.

Fig. 11, the effective diffusion coefficient given in Table 1 was employed, and the various equilibrium properties were chosen empirically to fit the band shape.

5.3. Volume overloading

Fig. 12 illustrates results from an experiment which investigates the effect of volume overloading on the protein band shape for the case where the feed slug size is 1.2 interstitial column void volumes. The experiment employs the same MES–acetate buffer system described previously, while the concentration of BSA was 1.0 mg ml^{-1} in the injection slug, which had a volume of 5.0 ml. As shown, good agreement was achieved between theory and experiment under these conditions. Furthermore, it can be seen that the width of the protein band when it exits the column is nearly the same in Figs. 8 and 12, which implies that the final protein band width is essentially indepen-
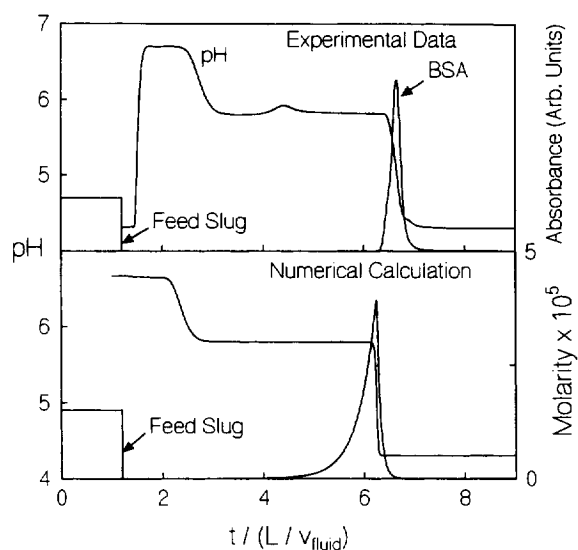

Fig. 12. Experimental data and numerical calculations for the chromatofocusing of BSA using a large volume feed slug. Experimental conditions and parameters for the numerical calculation are the same as in Fig. 8, except that the feed slug size is 5.0 ml and the flow-rate is 1.0 ml min^{-1}.

dent of the size of the feed slug under the conditions investigated.

6. Conclusions

The separation of dilute protein mixtures was achieved on a strong-base anion exchange column using internally generated pH gradients. Instead of using the synthetic polyampholyte buffers generally employed in chromatofocusing, a well-defined buffer system comprised of only a few buffering species was used to focus a target protein into a narrow band in the column effluent. The focusing behavior of proteins on internally generated stepwise pH transitions was shown to agree with numerical calculations based on independent measurements of pertinent physical properties, such as the intraparticle diffusivities and adsorption equilibrium parameters.

The chromatographic methods described here are able to focus large feed slugs into narrow bands, which allows large volumes of dilute protein mixtures to be concentrated and purified in a single chromatographic step. In addition, because of the large number of buffering species available (see, e.g.,

[19]), it is likely that the method can be used to separate and concentrate a wide variety of proteins. These qualities suggest that preparative-scale chromatofocusing methods of the type discussed here have the potential to increase throughput and decrease separation time for the downstream purification of proteins.

7. Symbols

A	Expression in square brackets in Eq. (3) $(cm^2 s^{-1})$
a_p	Parameter in Eq. (13)
C	Concentration in liquid phase $(g\,cm^{-3}$ or $mol\,cm^{-3})$
d_p	Particle diameter (cm)
D	Diffusion or axial dispersion coefficient $(cm^2 s^{-1})$
h	Reduced plate height
H	Height equivalent theoretical plate (cm)
K_t	Adsorption equilibrium coefficient per unit volume of particle
K_{ads}	Adsorption equilibrium coefficient per unit volume of adsorbed phase
k'	Capacity factor
L	Column length (cm)
n	Moles of solute in mobile phase per unit volume of column $(mol\,cm^{-3})$
$\bar{n}$	Moles of solute in adsorbed phase per unit volume of column $(mol\,cm^{-3})$
Pe_{AD}	Axial dispersion Peclet number
q	Concentration per unit volume of particle $(g\,cm^{-3}$ or $mol\,cm^{-3})$
q_{ads}	Concentration per unit volume of solid phase $(g\,cm^{-3}$ or $mol\,cm^{-3})$
q_R	Concentration of adsorbent function groups per unit volume of particle $(mol\,cm^{-3})$
t	Time (s)
t_0	Mean retention time of unadsorbed solute (s)
t_m	Mean retention time of solute (s)
v_{fluid}	Interstitial fluid velocity $(cm\,s^{-1})$
v_p	Velocity of protein band $(cm\,s^{-1})$
z_{ij}	Ratio of protein charge to exchanging ion charge $(z_{P_j}/z_{A_i^-})$
z_{P_j}	Charge on protein
$z_{A_i^-}$	Charge on negative form of buffering species

7.1. Greek symbols

α	Interparticle void volume fraction in bed
ϵ	Internal porosity of particle
ϕ_P	Column phase ratio $[((1-\alpha)(1-\epsilon_P))/(\alpha+(1-\alpha)\epsilon_P)]$

7.2. Superscripts and subscripts

ads	Adsorbed or solid phase
A or A_i	Buffering species i
AD	Axial dispersion
c	Combined value
eff	Effective value
P or P_j	Protein j
R	Adsorbent functional group
$-,0,+$	Negatively, uncharged, and positively charged forms of a buffering species
*	Equilibrium value

Acknowledgments

References

[1] L.A.Æ. Sluyterman and O. Elgersma, J. Chromatogr., 150 (1978) 17.
[2] L.A.Æ. Sluyterman and J. Wijdeness, J. Chromatogr., 150 (1978) 31.
[3] J.H. Scott, K.L. Kelner and H.P. Pollard, Anal. Biochem., 149 (1985) 163.
[4] M.T.W. Hearn and D. Lyttle, J. Chromatogr., 218 (1981) 483.
[5] D.D. Frey, A. Barnes and J. Strong, AIChE J., 41 (1995) 1171.
[6] D.D. Frey, Biotechnol. Progress, 12 (1996) 65.
[7] P.C. Wankat, Rate-Controlled Separations, Elsevier Applied Science, New York, 1990, p. 315.
[8] P.M. Boyer and J.T. Hsu, AIChE J., 38 (1992) 259.
[9] M.T.W. Hearn, A.N. Hodder, P.G. Stanton and M.I. Aguilar, Chromatographia, 24 (1987) 769.
[10] P. Schneider and J.M. Smith, AIChE J., 14 (1968) 762.

[11] A. Acrivos, Ind. Eng. Chem., 48 (1956) 703.

[12] A. Acrivos, Chem. Eng. Sci., 13 (1960) 1.

[13] S.F. Miller and C.J. King, AIChE J., 12 (1966) 767.

[14] R. Bird, W. Stewart and E. Lightfoot, Transport Phenomena, Wiley, New York, 1960, p. 514.

[15] R.D. Whitley, F.L. Wachter and N.-H.L. Wang, J. Chromatogr., 465 (1989) 137.

[16] R.K. Scopes, Protein Purification: Principles and Practice, Springer-Verlag, New York, 2nd ed., 1987, p. 109–110.

[17] C. Tanford, S.A. Swanson and W.S. Shore, J. Am. Chem. Soc., 77 (1955) 6414.

[18] R.V. Wenn and J. Williams, Biochem. J., 108 (1968) 69.

[19] H.A. McKenzie and R.M.C. Dawson, Data for Biochemical Research, Oxford University Press, London, 1969, pp. 475–508.